12-2022

Feasibility Analysis of Embedding Optical Fiber Sensor Into Additively Manufactured Part

Mahmudul Hasan Porag
The University of Texas Rio Grande Valley

FEASIBILITY ANALYSIS of EMBEDDING OPTICAL FIBER SENSOR INTO ADDITIVELY MANUFACTURED PART

A Thesis

by

MAHMUDUL HASAN PORAG

Submitted in Partial Fulfillment of the

Requirements for the Degree of

MASTER OF SCIENCE IN ENGINEERING

Major Subject: Manufacturing Engineering

The University of Texas Rio Grande Valley

December 2022

FEASIBILITY ANALYSIS of EMBEDDING OPTICAL FIBER SENSOR INTO ADDITIVELY MANUFACTURED PART

A Thesis
by
MAHMUDUL HASAN PORAG

COMMITTEE MEMBERS

Dr. Farid Ahmed
Chair of Committee

Dr. Jianzhi Li
Committee Member

Dr. Zhaohui Geng
Committee Member

December 2022

ABSTRACT

Porag, Mahmudul Hasan, Feasibility analysis for the embedment of Optical Fiber Sensors into Additively built Parts. Master of Science in Engineering (MSE), December, 2022, 37 pp., 8 tables, 37 figures, references, 40 titles.

The research tried to examine the viability of the embedment of optical fiber sensors in Additively built components, packaging the sensors within the components, and characterizing the sensors for sensing a specified measurement. Optical fiber sensors are popular due to their small size, resilience against electromagnetic radiation, and reliability in potentially dangerous conditions. Embedding fibers inside a product allows for the monitoring of critical areas, allowing for preemptive action in the case of a breakdown. Coupons of Inconel 718 were made using laser powder-bed fusion (LPBF), with the fabrication settings tuned to determine whether such a development was possible. After the FBG sensors were inserted in the channel, thermal epoxy was injected to seal the package. After the sample specimen was created, they were put through some tests like fatigue and thermal tests to determine their properties. This was done so that designers in the future would have a road map to follow when creating such a component, and so that we could learn whether the design was viable in general.

DEDICATION

My studies could not have been completed without the affection and support of my family and friends. My father, Md Abdul Jabbar, who has always given me good advice and supported me in all my decisions, and my sister, Jui, and Juthy, who believes in me unconditionally. My lab friends Forhad, Jabir, and Enrique whom I collaborated, and showed me about their culture through their amazing cooking and stories of their countries. Lastly, I would like to thank my friends for no particular reason other than being great friends and in no particular order: Riyad ,Bibhas, and Rashid.

ACKNOWLEDGMENTS

I am extremely grateful to Dr. Farid Ahmed, chair of my thesis committee, advisor, and professor, for guiding and mentoring me. I will forever be grateful to Dr. Jianzhi (James) Li, for believing in me and providing the resources needed for me to succeed. I would also like to thank my colleagues and friends at the lab who made my time at the lab a great experience. A special thank you to Dr. Robert Jones who was kind enough to help with fatigue testing. I would like to give my sincerest gratitude to Hernan who assisted me in carrying out the 3d printing process of my sample specimen.

TABLE OF CONTENTS

Page

LIST OF TABLES

Page

LIST OF FIGURES

Page

LIST OF FIGURES

Page

CHAPTER I

INTRODUCTION

Additive manufacturing is a process for being able to produce a three-dimensional solid from a digital model(Qin et al., 2017). Many companies in a variety of industries use additive manufacturing in their day-to-day operations, companies like these need to ensure that their products are being produced and are of the highest quality for customers. The integration of sensors such as fiber Bragg grating sensors into the system allows for the creation of smart structures to improve system performance and structural health monitoring(Son, 2021). Smart structures are used in a variety of applications, including composite materials that have embedded sensors, which allow users to detect and react to their surrounding environment in real-time(Munghen, 2021).

Through the integration of FBGs into materials, scientists can learn about the material's response to stresses like tensile and thermal loads. Normal strain in either tension or compression causes tensile stress to be generated in the material, which causes the FBG housed inside it to deform because of the strain(Son, 2021). Sensors are incorporated into 3D printed components as part of a layer-by-layer manufacturing process in order to create "smart" functioning items. One of the concerns for embedding sensors in the additively manufactured part is to examine how

printability problems and the constraints of the FBG sensors themselves are affecting the design of smart parts already on the market. The quality of the final component is dependent on machine settings, part shape, and orientation. In order to develop realistic and perfect samples, it is necessary to first select the optimal settings before doing any testing or other activities. It is necessary to take into account the direction of the fiber within the component since the application of FBGs in intricate geometries is constrained by the alignment of the FBGs. (Feng et al., 2015). Given that FBG sensors receive the most precise data when they are parallel to the direction of the strain, their use is restricted when the sensors' orientation is curved or misaligned(Li, 2007). In this project, additively manufactured were built and the sensor was embedded to analyze the feasibility of embedding sensor in 3D printed part. Fatigue and temperature tests were done to characterize the sensor data. The effect of different angles in the sample specimen channel is also considered to observe the efficient stress translation of the material to fiber optic sensor.

CHAPTER II

LITERATURE REVIEW

Sensors embedded in components provide real-time monitoring and control of system parameters. These sensors embedded components are referred to as smart components. Optical fiber sensors (OFS) have become more popular in the research field of structural health monitoring (SHM) for their capacity to measure a broad variety of physical parameters, their resistance to electromagnetic interference, and their mobility and embeddability. There is substantial research in the field of sensor embedding in additive manufacturing or relevant manufacturing processes. This section of the project will chronologically describe the development of the sensor embedding technology in the traditional and additive manufacturing processes and the limitation of the existing research.

As illustrated by Sandlin et al. FBGs can be embedded in Inconel 600 components using a vacuum brazing process. A satisfactory set of temperature and strain measurements has been made although Inconel 600 has a different thermal expansion coefficient than the fiber material. Additionally, a group of researchers (Li, 2007; Mihailov, 2012; Mrad et al., 1999) showed that ultrasonic additive manufacturing (UAM) is a method that may be used to assist the embedding of optical fibers in aluminum components. Along with the embedding approach, Schomer

provides extensive information on the characterization of embedded optical fibers, demonstrating the potential of embedded sensor components as well as the viability of using the UAM process to accomplish this goal. Fiber embedment into metallic objects in powder-based multilayer manufacturing has been shown for the first time by Li (Li, 2007). Based on a hybrid manufacturing method that alternated between additive – laser metal deposition (LMD) – and subtractive process phases, this technique was implemented. As a consequence of Li's Li (Li, 2007). achievements with the LMD technique, a number of other researchers have begun to consider the possibility of fiber embedding during many other manufacturing procedures. The integration of optical fibers into metallic objects during the Laser Powder Bed Fusion(L-PBF) process has recently seen a surge in the number of research work and publications devoted to this topic. Direct embedding of metallic coated fibers into stainless steel components on a Laser Powder Bed Fusion (L-PBF test setup has been described by Maier . In another study , Maier underscores the need of designing optical fiber sensors that can withstand the high heat loads encountered during direct L-PBF embedding. On an SLM test setup, Havermann discusses an embedment strategy for fiber optics into stainless steel coupons. Furthermore, he investigates the effects of different process variables on the embedment technique and the resulting bonding properties. Strain measurements on integrated fibers performed by Havermann reveal encouraging results. He took a step further and used the embedded fibers to quantify residual stresses in the L-PBF created components, which provides a better understanding of the L-PBF process and its properties. On the other hand, Mathew also did research on the issue, focusing on the integration of sensors that can monitor temperatures up to 1000 °C.It's evident from what

we've discussed so far that there are still certain issues that need to be addressed via more experiments and research. Creating a channel large enough for the sensors was a problem in past research. Previously, sensors were connected to the host material's surface, but this was not the best arrangement since it did not accurately represent the stress that the host material was under. As a result, it is preferable to place a sensor at or near the material's core. For this case, the strain transfer rate from the host material to fiber material is also a big concern as actual strain in the host material is not reflected in the fiber strain result. Additionally, when using FBGs with complicated geometry, it is important to consider the fiber orientation inside the channel. Because FBG sensors are most accurate when they are aligned with the strain, their application is restricted when the sensors are bent or misaligned, as the precision of the measurements decreases.

CHAPTER III

METHODOLOGY

At first, a sample specimen of the host material was fabricated in the 3D printing machine. The actual measurements of the sample specimen are 43.31 mm in length. For embedding sensors into the sample, specimen channels were created with varying diameters. During fabrication, it was planned that the length of the sample specimen must be as short as possible to avoid the complication of creating a high length-to-diameter ratio. Because of the narrow width of the channel, its length needs to be minimized. The length of the FBG patterns etched into the fiber is roughly 10mm. To allow for any possible movement of fiber within the coupon, its central region was made 12mm in length. The coupon's grasp section length was adjusted to 10mm on each side so that the tensile machine could securely hold the coupon.

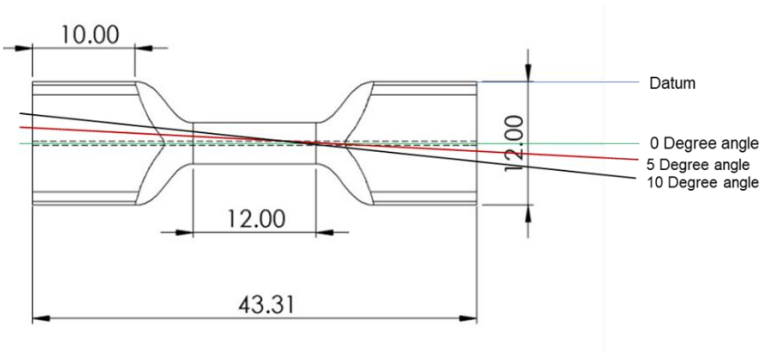

Figure 1 The specification of metal sample specimen

After printing the sample specimen, we need to embed the optical fiber sensor into it. During the embedment of the sensor we need to consider the diameter of the channel of the sample specimen. The samples were created using Laser Powder bed fusion process. For this experiment, the EOS M290 machine was used to create the 3d printed part. INCONEL 718 was chosen as the material due to its resistance to corrosion and it can withstand high pressure and temperature. Five different channel diameters (350 mm,450mm,550mm,650 mm, and 750mm) were created in the printing process. For each diameter, three different angles (0 degrees, 5 degrees, 10 degrees) were also created. The radius of the fiber that was used in the experiment is 125 microns. To insert the sensors into the channel of the sample specimen, the jacket of the fiber was taken away. So the final radius of the fiber was 62.5 microns. The creation of a narrow channel diameter is very crucial in this experiment as a melt pool is produced during the process of laser powder bed fusion and it can create blockage inside the channel. For a narrow channel, even a relatively small melt pool can have an effect along a sizable portion of its length. Additionally, the length of the specimen needs to be kept as small as possible because the greater the number of layers in the printing process, the more likely it is that the development of a melt pool will occur in channels with longer lengths. The large channel can also impact the translation of stress from the Inconel to the sensor. The translation of the stress must be accurate to get precise sensor data. The Bulk properties of the Inconel 718 is given below:

Table 1 Inconel 718 Bulk Properties

Property	Value	Unit
Poisson Ratio	0.284	
Density	8220	Kg/m^3
Young's Modulus	77.2	GPa
Coefficient of thermal expansion	7.2	10^-6 K
Thermal Conductivity	11.4	W/m-K

The fiber and the presence of a bonding mechanism are thought to require at least 300 microns channel size for the coupons. Accounting for the uneven/rough channel wall formation during the fabrication process, the minimum channel size planned for fabrication was 350 microns. To determine the smallest hole size usable for the study, various hole diameter sizes will be printed starting at 350 microns up to 750 microns. An experiment design for the Tensile test coupon for LPBF Printing is given below:

Table 2 Experiment Design for the Tensile test coupon for LPBF Printing

Channel Diameter	350 mm	Angle (Degree)	0
			5
			10
	450 mm	Angle (Degree)	0
			5
			10
	550 mm	Angle (Degree)	0
			5
			10
	650 mm	Angle (Degree)	0
			5
			10
	750 mm	Angle (Degree)	0
			5
			10

Beside the experimental design, a theoretical mathematical model was done using python to understand the influence of different angle for the strain transfer rate of the host material to optical fiber sensor from a previous literature(Li, 2007). The Mechanical properties of the optical fiber and interlayer for the model are given below:

Table 3 Mechanical properties of the optical fiber and interlayer

Material parameters	Symbol	Value	Unit
Young's modulus for the glass fiber	*Eg*	7.2*10^10	Pa
Young's modulus for the interlayer	*Ec*	2.6*10^10	Pa
Poisson ratio of the interlayer	vc	0.48	-
Radius of the outer boundary of the interlayer	rm	102.50	um
Radius of the glass fiber	rg	62.50	um

After the coupon had been created, it was placed inside a beaker that was full of acetone and then placed inside ultrasonic cleaning equipment for a period of half an hour. In that machine, ethanol was agitated through ultrasonic waves in order to clean printed coupons. The ultrasonic cleaning was to ensure that the coupon's channel was free of any leftover detritus. To achieve a high level of reading precision with the FBG-Coupon system, the bonding mechanism must transfer the axial strain to the epoxy from the material of the sample specimen in a efficient manner. This is because the host material must be capable of efficiently translating the stress that is being experienced to the FBG in order to obtain the most precise measurements. Based on the findings of this research, polymer-based epoxy was identified as the choice for the specified purposes. This is because of their superior fatigue and mechanical strength as well as the

shrinkage rate is relatively low after curing. Figure 3.4 depicts the conceptualization of the FBG-Coupon assembly, in which the fiber would be centered on the neck of the coupon and pass entirely through it. We bonded the INCONEL 718 to the FBG using Infinity Bond's EP-3530ND Optical Epoxy, as mentioned in the literature review. This is due to the fact that the EP-3530ND is used in high-temperature fiber optic applications.

This epoxy is a two-component system with a recommended mixing ratio of 10 parts hardener to 1 part hardener. Substrates were distributed uniformly by placing each component in its own beaker and stirring for one minute. After that, they were combined in one beaker and given a further minute of stirring.

When The depth at which the fiber had to be inserted into the channel had previously been marked, as the grating section of the fiber (10 mm in length) had to be in the middle of the sample specimen to get the precise measurement. After that the jacket of the senor will be removed so that the transfer of the stress from host material to fiber core need less distance. The sensor with jacket was submerged in acetone for 5 minutes to remove the jacket. The process summarized below:

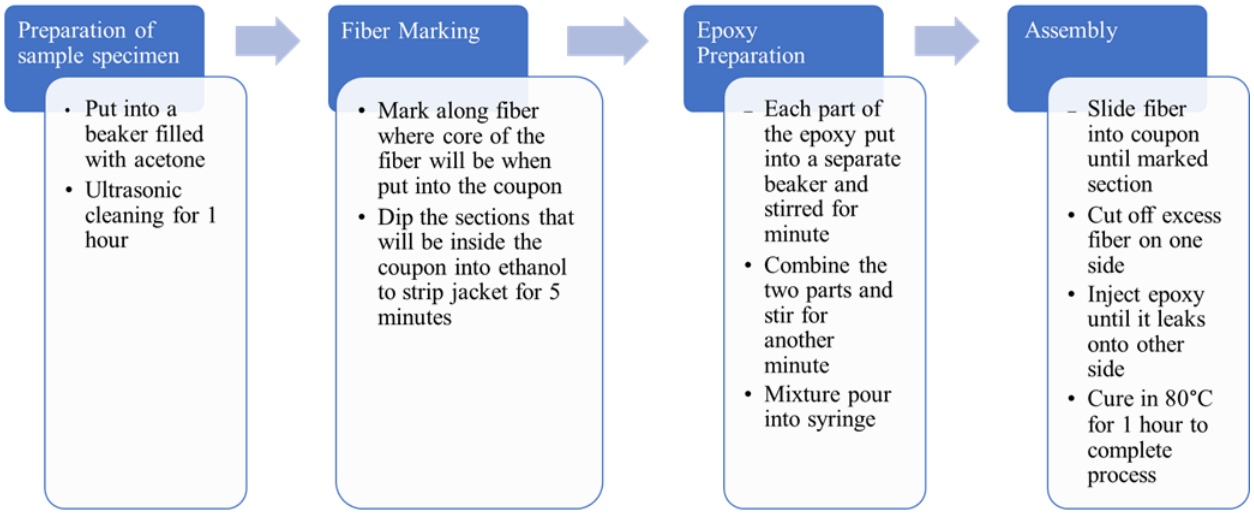

Figure 2: Summary of sensor embedding process

To put sensor is centered in the sample specimen, the fiber was inserted into the channel all the way to the designated position. After the marks have been aligned with the coupon's border, the surplus fiber at the opposite end is snipped off. Thus, the fiber would run parallel to the full coupon's width. After trimming the superfluous fiber, the epoxy mixture was placed into a syringe with a 350-micron needle and inserted into the channel. It was crucial to keep the sample specimen and fiber in place since the injected epoxy has the potential to push the fiber away from the channel if it moves. It took around 5 minutes since the epoxy was so thick that it had to be discharged from the syringe and travel the whole length of the channel. The syringe was supposed to be taken away once it was observed that epoxy was dripping out of the opposite end of the channel. After that the sample specimen with embedded sensor was cured on a hot plate by holding the temperature around 80°. After the FBG had been encased in epoxy and

placed inside the coupon, the entirety of the assembly needed to be prepared before the FBG's wavelength spectrum could be analyzed.

The FBG-containing coupon is scanned by an optical interrogator, which is linked to the fiber that emerges from the coupon. The FBG sensor may be monitored in both static and moving environments with the help of the optical interrogator. The interrogator uses an optical source with a sweeping wavelength to transmit light down the wire. By sensing and processing the light wavelength reflected to the unit, the FBG may obtain spectral data . Micron Optics' HYPERION optical sensing unit si155 was the optical interrogator utilized in the experiment. For its adaptable peak-detection technique, this interrogator came out on top. Users are given the freedom to adjust the currently selected peak. Some peaks faded or changed form as the sensors were exposed to different environments. The detectable peaks were narrowed down thanks to the detectable peaks' flexibility. Also, an ethernet cable links the optical interrogator to a computer. To operate and fine-tune the optical interrogator, a computer with the ENLIGHT software loaded is required.

Here, we discuss the tests developed to learn about the sensor's behavior under different conditions, like thermal and mechanical stress. In the next sections, we'll go over the various test cases and how they were set up. The impacts of tensile stress, thermal stress, and angular channel on the FBG spectrum were the focus of this study.

The coupon will be subjected to a series of stresses in an effort to determine how those stresses will manifest in the spectrum. These findings provide a benchmark from which to

compare future wavelength measurements. Here, the coupon containing the FBG was meant to be put through a tensile stress machine. The stress and strain values of the coupon were recorded from the tensile stress machine's output. In order to characterize the fiber, this value was supposed to be compared to the FBG's spectral reading. Since the FBG sensor is situated at the neck of the coupon and the neck would be the cracking area in a tensile test, this is the region of interest.

Again, it was cut into various pieces for tensile testing, with the goal of investigating three distinct tensile loading conditions. The first step was to calculate the FBG-Coupon assembly's elastic limit in order to establish the maximum stress that can be applied to the FBG sensor assembly without causing irreparable damage (plastic deformation). The next step is a cyclic loading scenario, and ultimately a failure test in which the coupon is stretched until no further FBG signals can be detected. The sensors will be characterized using a combination of cyclic testing and a failure test.

Fatigue test was designed to check whether the wavelength would revert to original state after several cycles. This experiment is valuable because knowing the coupon's repeatability and the FBG's lifespan helps determine whether the technology can be successfully implemented in smart devices. The full procedure is described below:

Figure 3: Sample set up in the fatigue testing machine

The primary goal of this experiment is to examine how temperature affects the sensitivity of FBG sensors. With this evaluation, you can observe how the sensor performs throughout a wide temperature spectrum and in fine-grained increments. By conducting this evaluation, we can learn how reliable and stable the FBG assembly is. The FBG-encased Inconel coupon was heated and cooled to different degrees to begin characterization. The set up for the thermal test is given in the following figure:

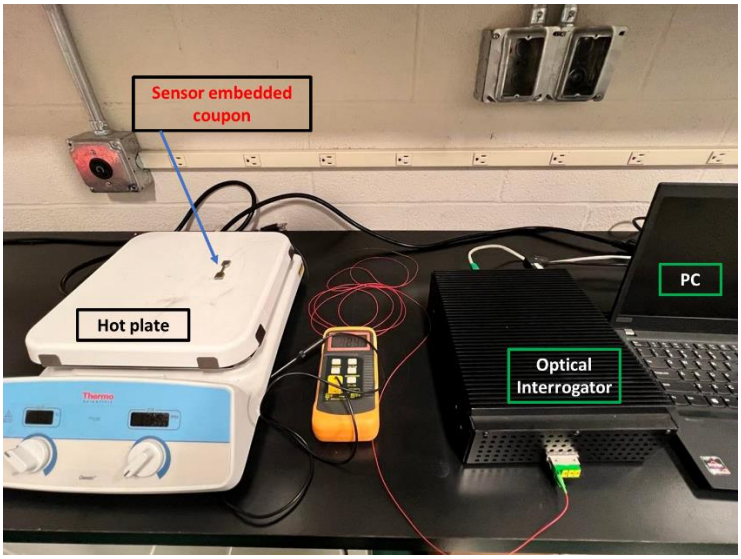

Figure 4: Set up for the thermal testing of sensor embedded sample

To get the most reliable findings, the sample was kept on the hotplate around 4 hours to bring the temperature of the inside of the coupon up to that of the surface. An first heating to a predetermined temperature was followed by a ten-minute hold at that temperature before the embedded assembly was heated once more. After each change, the temperature was maintained for 10 minutes to ensure that the readings had a chance to settle and reach equilibrium. During preliminary thermal testing, it was hypothesized that the epoxy in its elevated temperature state may alleviate some residual tension inside the channel.

Right now, the epoxy is the test's bottleneck because it can't withstand temperatures above 300 degrees Celsius. The wavelength of raw FBG expands by 10 picometers for every 1 degree Celsius when it is heated. Considering that the FBG is now housed behind a stainless-steel coupon, observing the effects of this change could prove interesting.

CHAPTER IV

RESULT & DISCUSSION

The fabrication of sample specimen was successfully done on EOS M290 machine. Coupons were printed using the EOS M290 machine's default settings. The following diagram displays the outcomes of this method for clearing channels of varying widths. Under 550 mm in channel diameter, full clearance was not possible.

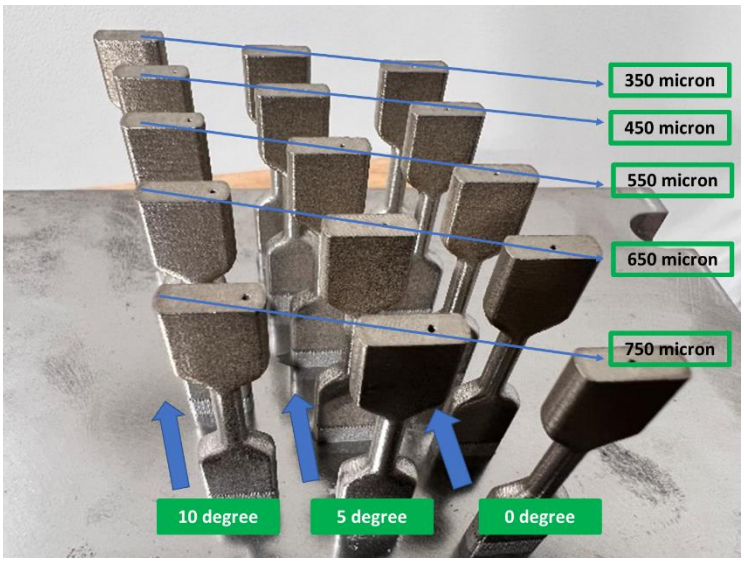

Figure 5: Successfully Printed coupons

To have better clearance of the channel some post-processing was performed. At first the sample specimen were polished using grit paper. After that the sample specimen were taken in an acetone solution to clean the debris or any other particles present in the channel. The image analysis of the channel clearance is described in the following figures :

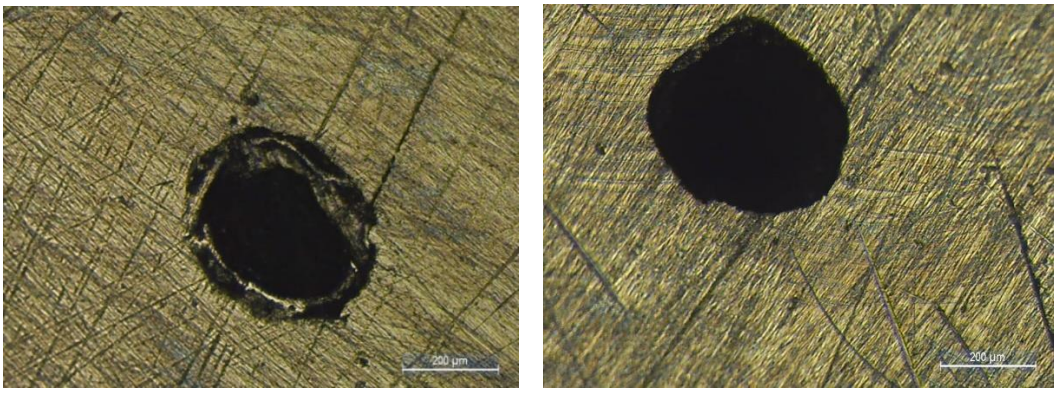

Figure 6: Optical image of the channel (350 microns) before sensor embedding

From the above figures it can be seen that, the there is lack of full clearance in the channel and also the hole is not perfectly round. Almost similar result happens in the 450-micron channel. As we are aiming to have a narrow channel, our next target was to embed the sensor in the 550-micron channel coupon. The sample coupon was marked both sideways and also on the top surface during cutting. The sideways marking was done to cut the sample in the same direction so that we can understand the picture from a specific direction. The top surface marking was done to make a specific interval of the gauge length for cutting. The optical image of sensor embedded specimen is also described below:

Figure 7 : Sample specimen with marking for cutting

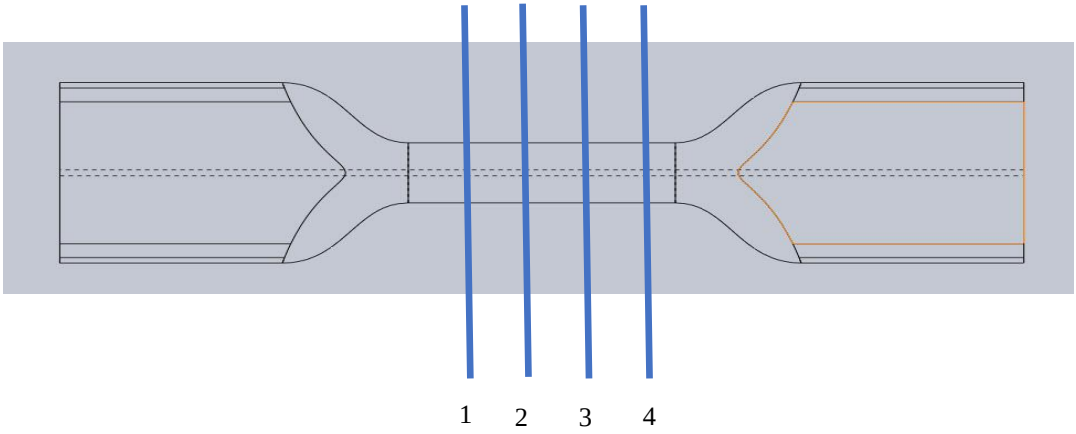

Figure 8: Schematic of sensor embedded coupon with marking

1

The images of sensor embedded coupon give us insightful information. The sensor is visible in the picture and the presence of materials in the channel diameter is also observed. The interesting fact is that one of the pictures (No. 2) showed that the location of the sensor in the channel is very crucial. If the sensor is very near to the channel, it can cause pinching in the channel wall and thus causing damage in the sensor. So we have to very careful during the embedding process to place the sensor not very close to the channel wall.

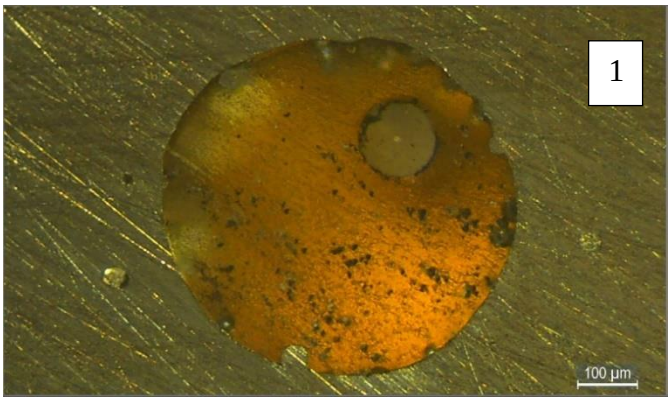

Figure 9: Optical microscope picture of sensor embedded channel

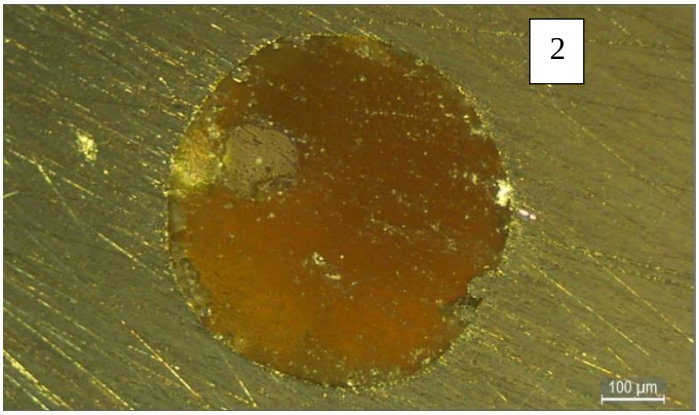

Figure 10: Optical microscope picture of sensor embedded channel

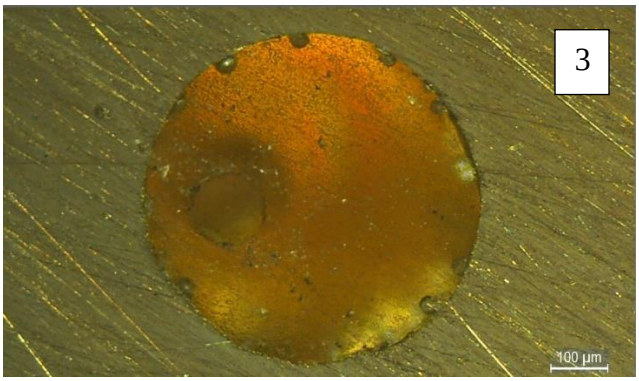

Figure 11: Optical microscope picture of sensor embedded channel

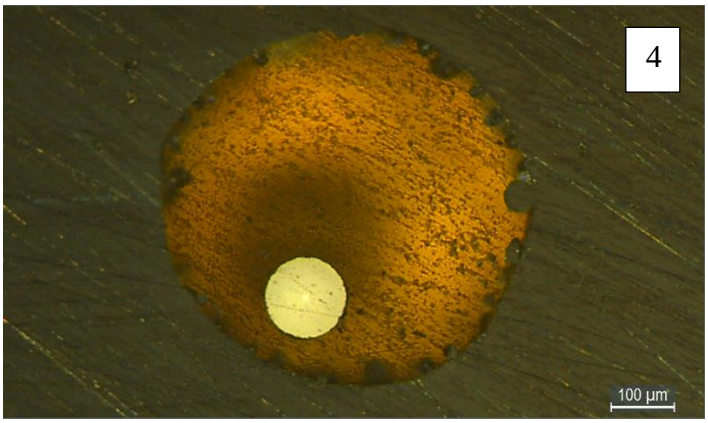

Figure 12: Optical microscope picture of sensor embedded channel

It was planned to embed the fiber into the perfect coupon after the coupon was generated. As was previously agreed upon, the bonding technique of choice is Infinity Bond's 3530ND Optical Epoxy. It's important to leave enough space for the epoxy to cure and expand during thermal processing ; otherwise, the FBG could experience internal strain.

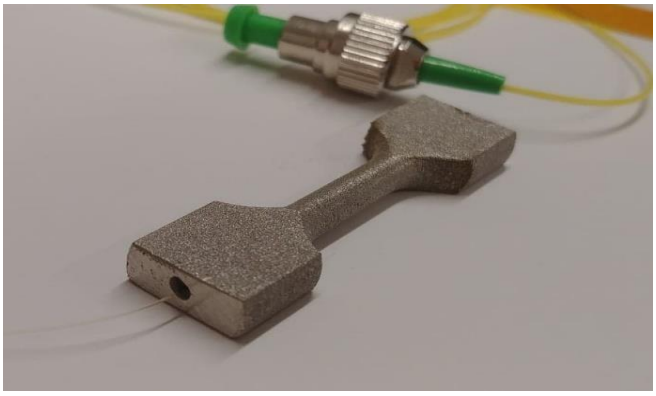

Figure 13: Sensor embedded sample specimen

This successful integrated coupon is shown in the above figure. The cured epoxy leaves a black residue at the coupon's bottom, which is where the fiber is sticking out. The embedded assembly was cured in a hot plate at 80-degree celcius for half an hour.

For fatigue testing we used three sample specimens 0-degree, 5 degree, 10 degree with 550 micron channel diameter. For each sample there were three blocks of experiment run. The process was described in the previous section. The graphs will discuss the material response of the sensor due to fatigue loading (base load and cyclic load).

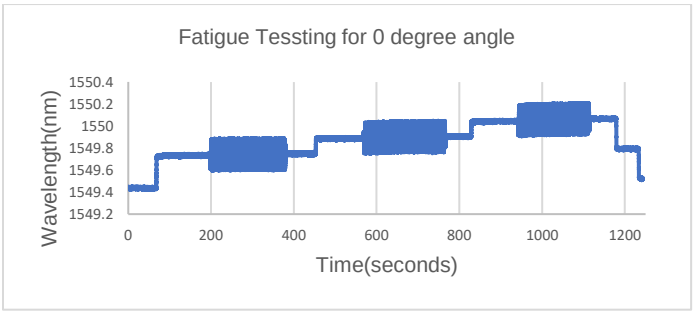

Figure 14: fatigue testing for 0-degree angle

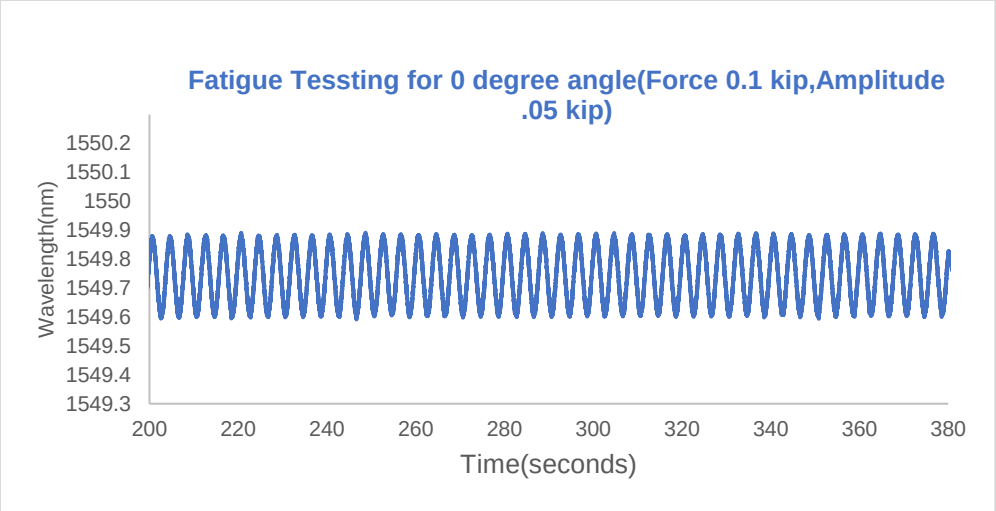

Figure 15: fatigue testing for 0-degree angle (Force 0.1 kpi, amplitude .05 kpi)

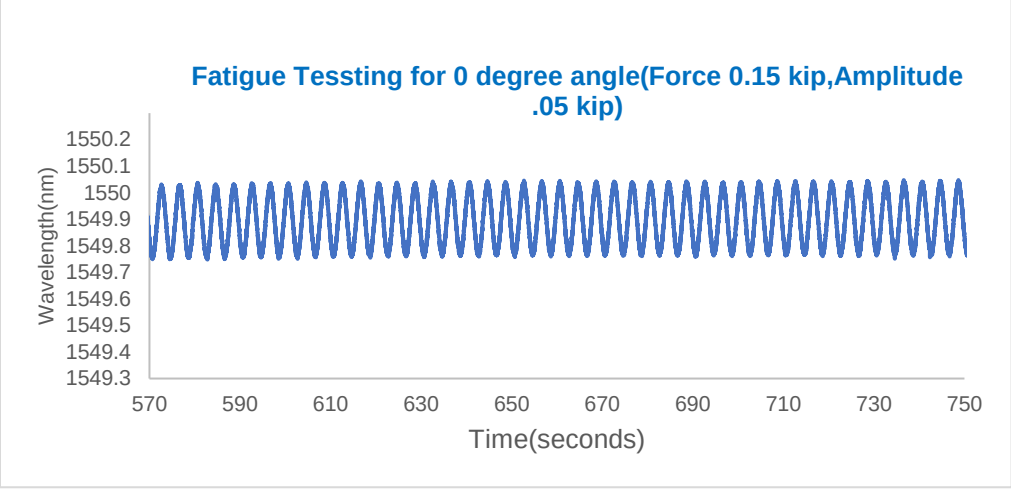

Figure 16: fatigue testing for 0-degree angle (Force 0.15 kip, amplitude .05 kip)

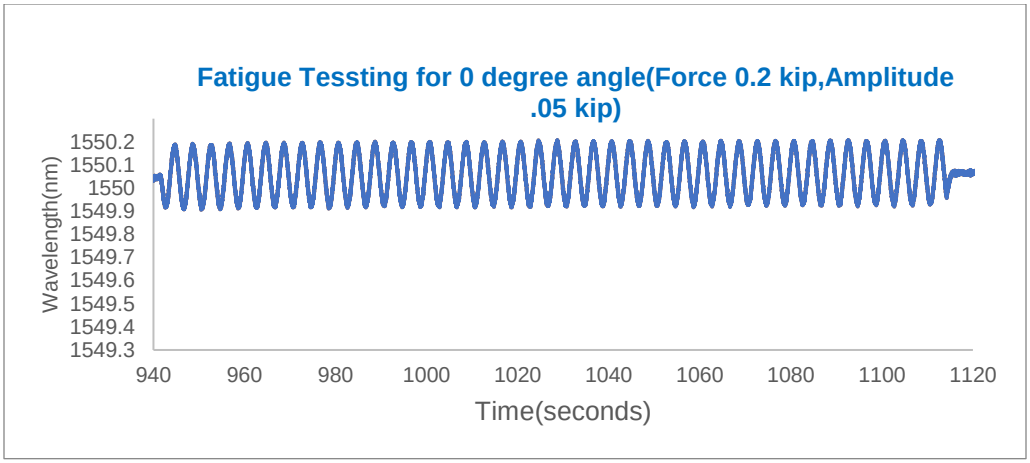

Figure17: fatigue testing for 0-degree angle (Force 0.2 kip, amplitude .05 kip)

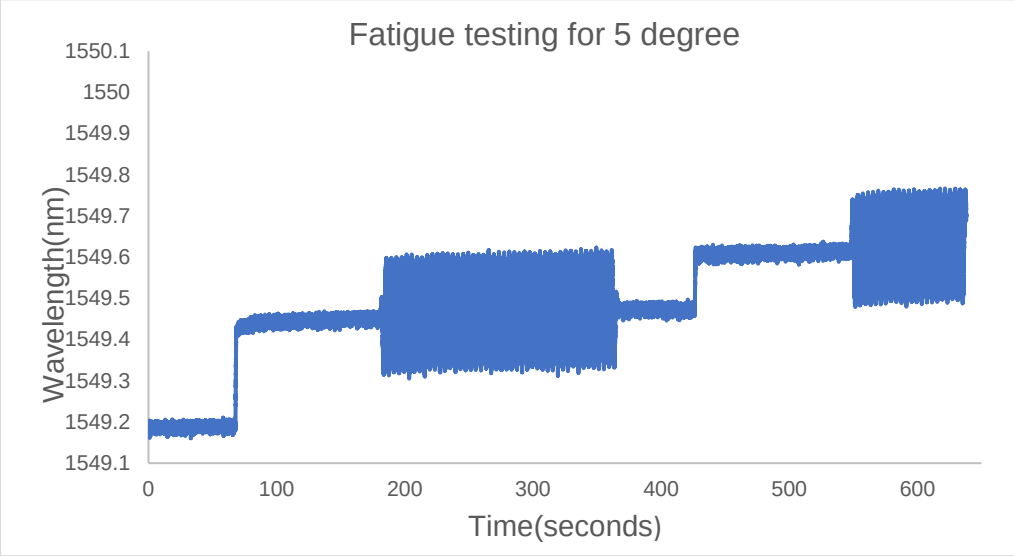

Figure 18: fatigue testing for 5-degree angle

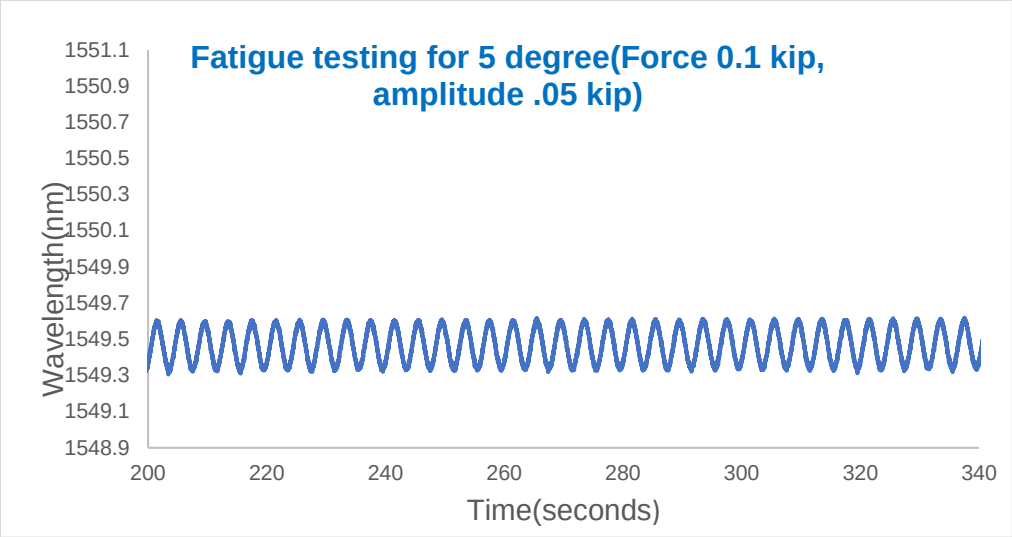

Figure 19: fatigue testing for 5-degree angle (Force 0.1 kip, amplitude .05 kip)

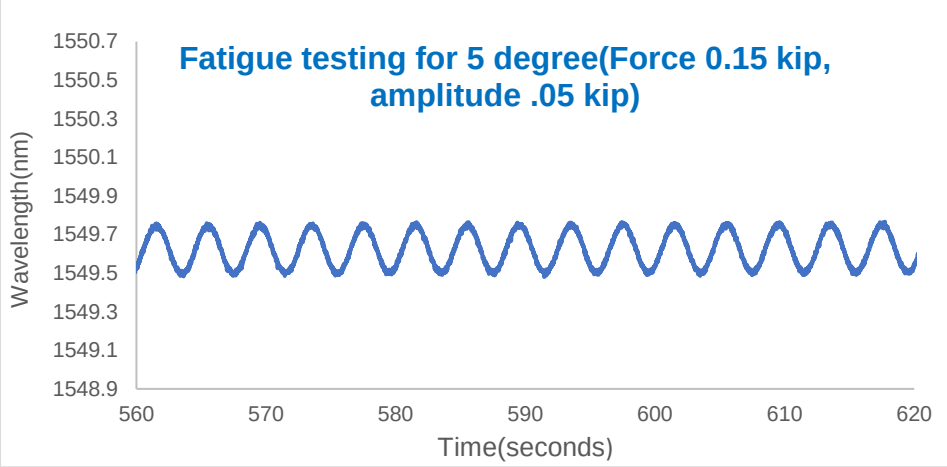

Figure 20: fatigue testing for 5-degree angle (Force 0.15 kpi, amplitude .05 kpi)

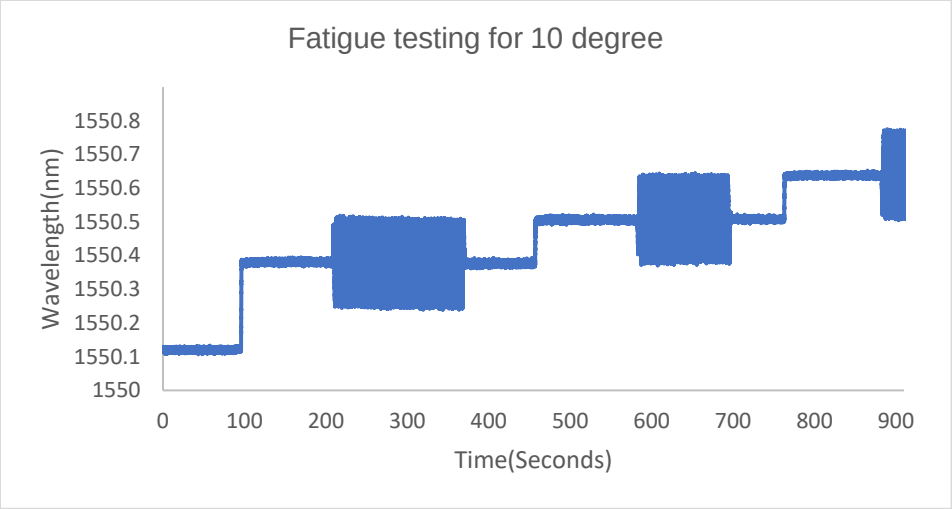

Figure 21: fatigue testing for 10-degree angle

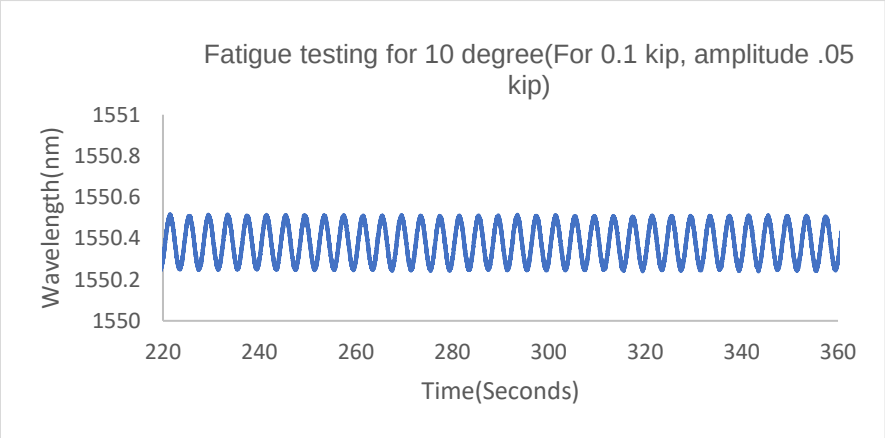

Figure 22: fatigue testing for 10-degree angle (Force 0.1-kip, amplitude .05 kip)

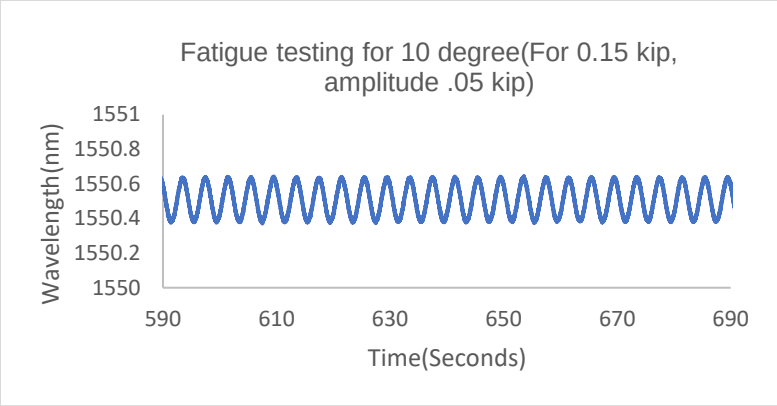

Figure 23 : fatigue testing for 10-degree angle (Force 0.15 kip, amplitude .05 kip)

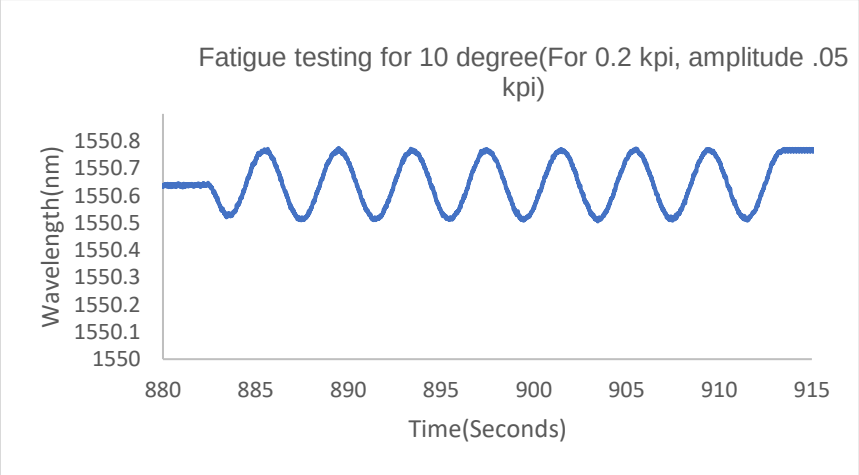

Figure 24: fatigue testing for 10-degree angle (Force 0.2 kpi, amplitude .05 kpi)

The result from the fatigue test ensures the repeatability and replicability of the sensor data. The data found in the results shows the material response of the sensor embedded coupon for various load and cyclic loading. For the cyclic loading section, it is found that the wavelength deviation also follows the sine wave. The wavelength shift for varying fatigue load (0.1 kip,0.15 kip,0.2 kip) with different angles (0 degree, 5 degree, 10 degree) was analyzed to observe the

behavior of the sensor data. The data was extracted from Enlight software. In the following figure the wavelength shift for the sample specimen is shown. It can be seen that for each load the wavelength was shifted to the right. That indicates the response of the sensor due to the load applied on the fatigue machine. The greater load the wavelength shifted to the rightward with reference to the initial spectrum.

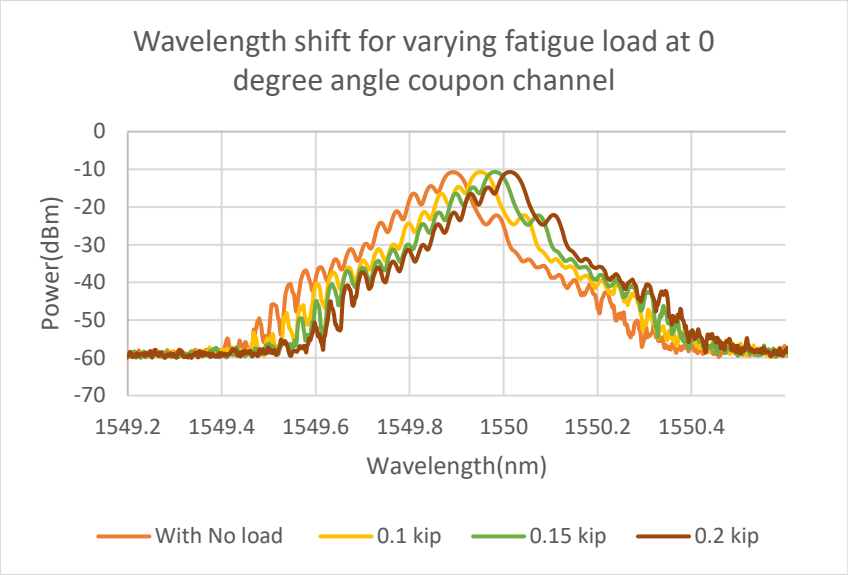

Figure 25: Wavelength shift for varying fatigue load at 0 degree channel

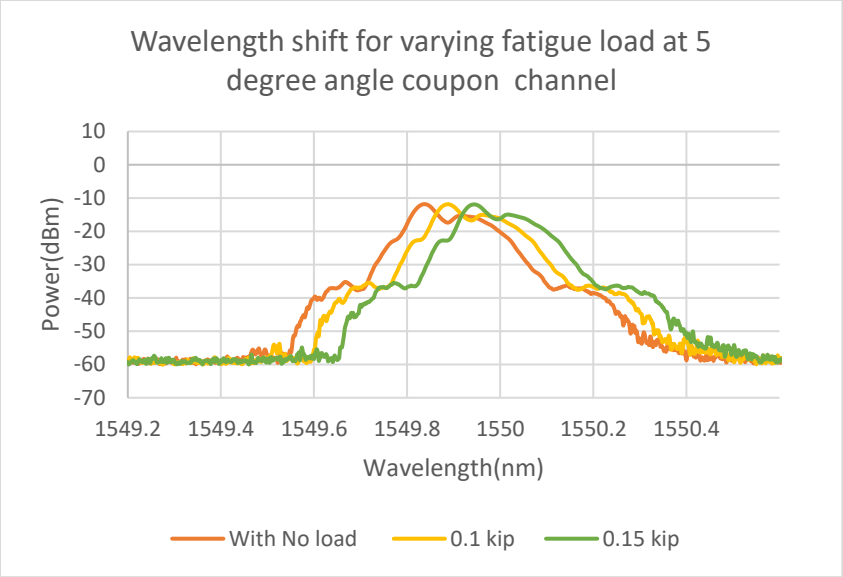

Figure 26: Wavelength shift for varying fatigue load at 5-degree channel

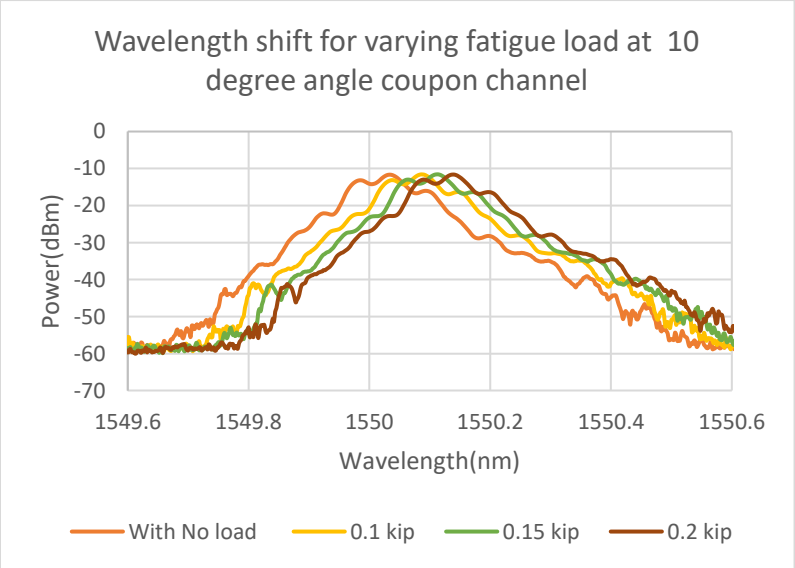

Figure 27: Wavelength shift for varying fatigue load at 10-degree channel

The average wavelength shift for varying fatigue load is observed in the following figure. The wavelength shift is very prominent for 0 degree and for 5 degree and 10 degree it is almost similar. It can be observed that the greater the angle of the force with the sensor channel the less the wavelength shift of the fiber. It indicates that the angle has an impact for the stress translation from host specimen to sensor. For 0-degree coupon channel the stress translation is easier than the channel with an angle.

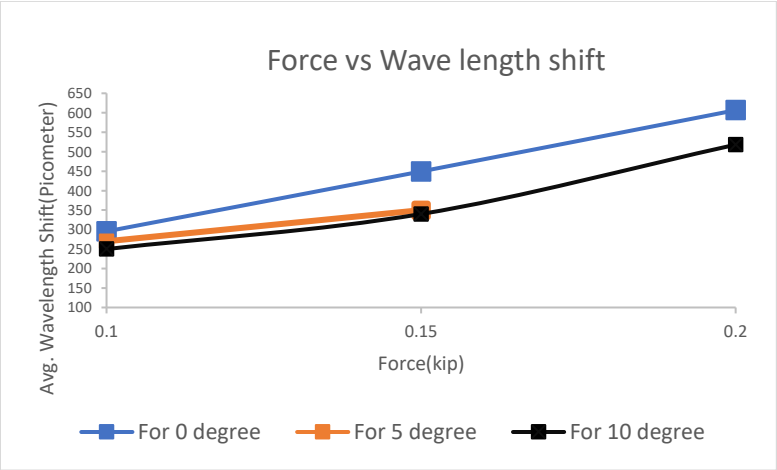

Figure 28: Force vs Average wavelength shift

In the previous figure we observed the wavelength shift for the base load. Now for the cyclic loading condition the average spectrum height was observed. Normally the height of 0 degree is higher than the other angle. Additionally, it is observed that the as the time increases the average height of the spectrum is decreasing for all block of cyclic loading.

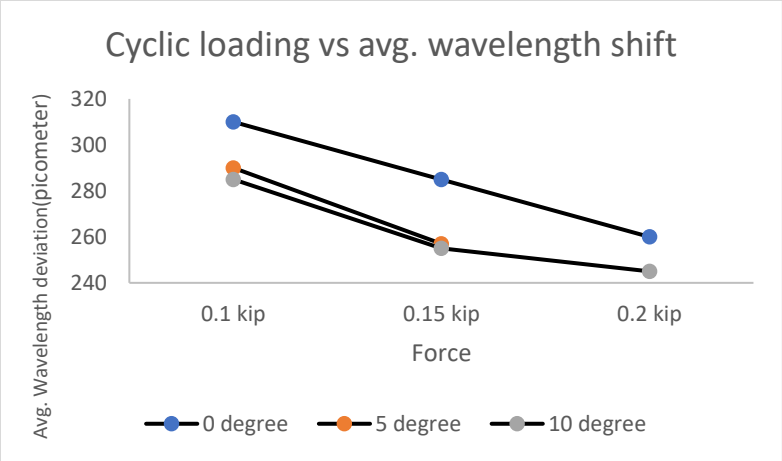

Figure 29: Force (cyclic loading) vs avg. wavelength shift

The thermal test shows that the wavelength is increasing with the increased temperature. In the experiment we increased the temperature and hold for 25 minutes to stabilize the temperature in the hot plate. The wavelength increases when the temperature is increased and after 4-5 minutes it gives same wavelength. The following pictures shows the wavelength shift with respect to time during different temperature:

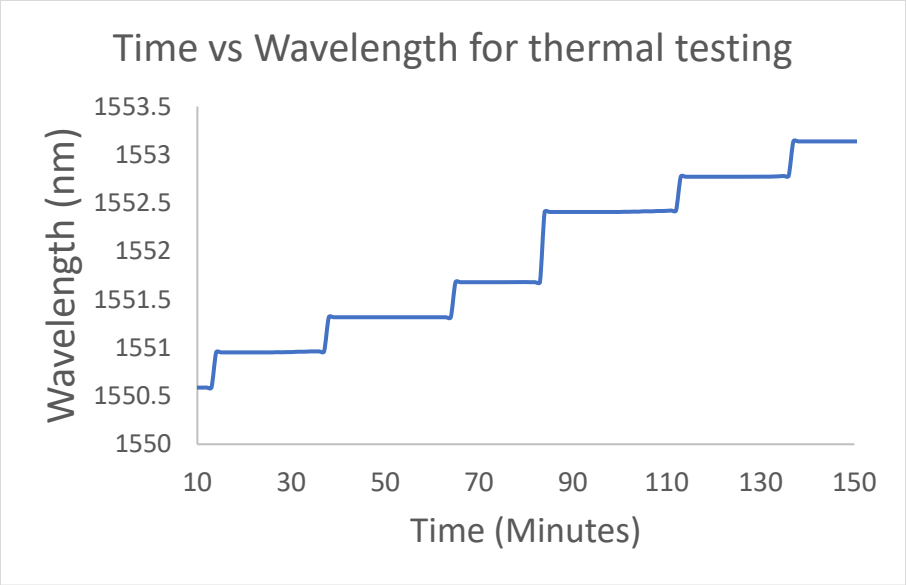

Figure 30: Time vs Wavelength graph for thermal test

The sensitivity of the temperature for the sensor embedded coupon is also observed with the bare sensor . It is observed that the wavelength deviation is increasing with the increased temperature for both bare and embedded sensors. The sensitivity for embedded coupon is much higher than the bare sensor. The sensitivity for embedded sensor is around 36.4 picometer per degree celcius. On the other hand, the sensitivity for the bare sensor is approximately 11 picometer per degree celcius.

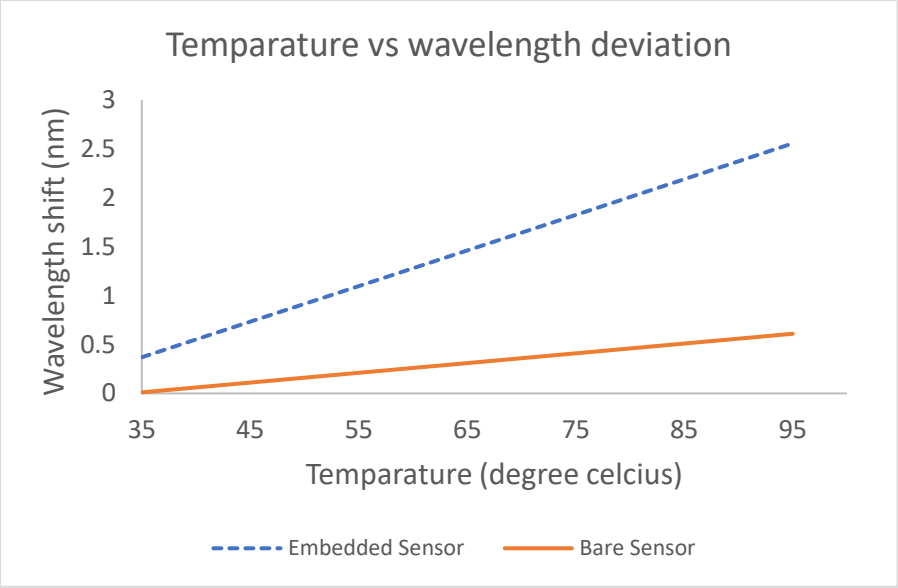

Figure 31: temperature vs wavelength shift

CHAPTER V

CONCLUSION

This research endeavored to discover the feasibility of including sensors into additively built metal components for the purpose of creating smart products. To take application-specific specimen measurements with metal Additive Manufacturing (AM), one must overcome the difficulties of both building suitable channels (for sensor embedding) and packing the sensor in an AM product. For the most part, optical fiber sensors have been favored because of their small form factor, reliability in potentially dangerous situations, and resistance to electromagnetic radiation.

When doing similar work in the future, it is suggested that you try using a different material for sample specimen as well as epoxy. By doing so, one can acquire a deeper set of rules and information for developing innovative product ideas. The designer will have more options to consider in terms of material and epoxy with a more comprehensive guideline. More experiments of varying curvature angles will provide a more comprehensive picture of how curvature affects peak wavelength measurement.

REFERENCES

Aggogeri, F., Borboni, A., Faglia, R., Merlo, A., & Pellegrini, N. (2017). A kinematic model to compensate the structural deformations in machine tools using fiber Bragg grating (FBG) sensors. *Applied Sciences*, *7*(2), 114.

Ansari, F., & Libo, Y. (1998). Mechanics of bond and interface shear transfer in optical fiber sensors. Journal of engineering mechanics, 124(4), 385-394.

Botsis, J., Humbert, L., Colpo, F., & Giaccari, P. (2005). Embedded fiber Bragg grating sensor for internal strain measurements in polymeric materials. Optics and lasers in Engineering, 43(3-5), 491-510.

Canal, L. P., Sarfaraz, R., Violakis, G., Botsis, J., Michaud, V., & Limberger, H. G. (2014). Monitoring strain gradients in adhesive composite joints by embedded fiber Bragg grating sensors. Composite Structures, 112, 241-247.

Cusano, A., Capoluongo, P., Campopiano, S., Cutolo, A., Giordano, M., Felli, F., ... & Caponero, M. (2006). Experimental modal analysis of an aircraft model wing by embedded fiber Bragg grating sensors. IEEE Sensors Journal, 6(1), 67-77.

Dhavamani, V., Chakraborty, S., Ramya, S., & Nandi, S. (2022). Design and Simulation of Waveguide Bragg Grating based Temperature Sensor in COMSOL. In Journal of Physics: Conference Series (Vol. 2161, No. 1, p. 012047). IOP Publishing.

Di Sante, R., & Donati, L. (2013). Strain monitoring with embedded Fiber Bragg Gratings in advanced composite structures for nautical applications. Measurement, 46(7), 2118-2126.

Fedorov, A. Y., Kosheleva, N. A., Matveenko, V. P., & Serovaev, G. S. (2020). Strain measurement and stress analysis in the vicinity of a fiber Bragg grating sensor embedded in a composite material. Composite Structures, 239, 111844.

Huang, J., Zhou, Z., Liu, M., Zhang, E., Chen, M., Pham, D. T., & Ji, C. (2015). Real-time measurement of temperature field in heavy-duty machine tools using fiber Bragg grating sensors and analysis of thermal shift errors. Mechatronics, 31, 16-21.

Li, D., Ren, L., & Li, H. (2012). Mechanical property and strain transferring mechanism in optical fiber sensors. IntechOpen.

Li, D. S., Li Sr, H., Ren, L., & Song, G. (2006). Strain transferring analysis of fiber Bragg grating sensors. Optical Engineering, 45(2), 024402.

Li, H. N., Zhou, G. D., Liang, R., & Li, D. S. (2007). Strain transfer analysis of embedded fiber Bragg grating sensor under nonaxial stress. Optical Engineering, 46(5), 054402.

Pak, Y. E. (1992). Longitudinal shear transfer in fiber optic sensors. Smart materials and structures, 1(1), 57.

Prabhugoud, M., & Peters, K. (2004). Modified transfer matrix formulation for Bragg grating strain sensors. Journal of lightwave technology, 22(10), 2302.

Serovaev, G., Matveenko, V., Kosheleva, N., & Fedorov, A. (2019). Numerical modeling of the capillary in the Bragg grating area, ensuring uniaxial stress state of embedded fiber-optic strain sensor. Procedia Structural Integrity, 17, 371-378.

Silva-Muñoz, R. A., & Lopez-Anido, R. A. (2009). Structural health monitoring of marine composite structural joints using embedded fiber Bragg grating strain sensors. Composite Structures, 89(2), 224-234.

Yao, K., Lin, Q., Jiang, Z., Zhao, N., Tian, B., Shi, P., & Peng, G. D. (2018). Modeling and analysis of a combined stress-vibration fiber Bragg grating sensor. Sensors, 18(3), 743.

Zaitsev, I. O., Shpylka, A., & Shpylka, N. (2020, February). Output signal processing method for fiber bragg grating sensing system. In 2020 IEEE 15th International Conference on Advanced Trends in Radioelectronics, Telecommunications and Computer Engineering (TCSET) (pp. 152-155). IEEE.

Zheng, Y., Zhu, Z. W., Deng, Q. X., & Xiao, F. (2019). Theoretical and experimental study on the fiber Bragg grating-based inclinometer for slope displacement monitoring. Optical Fiber Technology, 49, 28-36.

BIOGRAPHICAL SKETCH

Mahmudul Hasan Porag completed his Master of Science degree in Manufacturing Engineering at the University of Texas Rio Grande Valley in December 2022. He received his B.Sc. in Industrial Engineering from Bangladesh University of Engineering and Technology. He completed his Master of Science degree in Engineering Management at the University of Texas Rio Grande Valley in December 2022. He had 5 years of experience in manufacturing, supply chain, lean six sigma. He can be reached at porag024@gmail.com.